

Rapid evolution of [WC] stars in the Magellanic Clouds[★]

Marcin Hajduk¹

Space Radio-Diagnostics Research Centre, University of Warmia and Mazury, ul.Oczapowskiego 2, 10-719 Olsztyn, Poland
e-mail: marcin.hajduk@uwm.edu.pl

Received September 15, 1996; accepted March 16, 1997

ABSTRACT

We obtained new spectra of fourteen Magellanic Cloud planetary nebulae with the South African Large Telescope to determine heating rates of their central stars and to verify evolutionary models of post-asymptotic giant branch stars. We compared new spectra with observations made in previous years. Five planetary nebulae showed an increase in excitation over time. Four of their central stars exhibit [WC] features in their spectra, including three new detections. This raises the total number of [WC] central stars of PNe in the Magellanic Clouds to ten. We compared determined heating rates of the four [WC] central stars with the He-burning post-asymptotic giant branch evolutionary tracks and the remaining star with the H-burning tracks. Determined heating rates are consistent with the evolutionary models for both H and He-burning post-asymptotic giant branch stars. The central stars of the PNe that show the fastest increase of excitation are also the most luminous in the sample. This indicates that [WC] central stars in the Magellanic Clouds evolve faster than H-burning central stars, and they originate from more massive progenitors.

Key words. planetary nebulae: general — stars: AGB and post-AGB — stars: evolution

1. Introduction

Stars with initial masses in the range of $1 - 8 M_{\odot}$ lose most of their envelope on the asymptotic giant branch (AGB). During an early AGB phase, helium burning proceeds in a thin shell on the top of the carbon-oxygen core. When the helium shell reaches the hydrogen shell, the nuclear burning becomes unstable. A series of helium shell flashes punctuate quiescent hydrogen burning.

The large energy generation due to a helium flash induces a convective instability between the shells (Iben & Renzini 1983; Herwig 2005). When the H shell becomes active again, part of the intershell material is dredged up to the surface.

The envelope of the star is rapidly expelled due to the intensive mass loss experienced during the AGB phase. This reduces the number of helium shell flashes. The mass ejected by AGB stars significantly contributes to the chemical evolution of galaxies and stellar systems (Karakas 2010).

After a star ejects most of its envelope, it terminates the AGB phase and its evolution accelerates. Heating rate increases from $\dot{T}_{*} \lesssim 0.1 \text{ kK yr}^{-1}$ to $1 \text{ K yr}^{-1} \lesssim \dot{T}_{*} \lesssim 10 \text{ kK yr}^{-1}$ (Miller Bertolami 2019). The evolutionary timescale of post-AGB stars is a very strong function of their envelope mass and the nuclear burning rate. Post-AGB stars occupy a relatively narrow range in mass between 0.5 and $0.9 M_{\odot}$, but evolutionary timescales differ by a few orders of magnitude within this range.

Post-AGB stars cross the H-R diagram from low to high temperatures almost at constant luminosity, as long as the shell sources remain active (Paczynski 1970). Once the star is hot enough, the ionization front expands throughout the shell ejected during the AGB phase. The shell forms a planetary nebula (PN).

The excitation of the PN increases with the increasing temperature of the central star.

A central star of a PN may experience a final thermal pulse after it leaves AGB (Schoenberger 1979). A final thermal pulse can punctuate evolution of a post-AGB star immediately after it leaves the AGB (called AFTP), during its horizontal evolution, when H-burning shell is active (late thermal pulse - LTP), or during cooling (very late thermal pulse - VLTP) (Koesterke 2001).

In the result of the VLTP, the pulse driven convecting zone eventually reaches out into the H-rich envelope (Herwig 2005). The LTP and AFTP lead to the diluted shell and significantly reduced H abundance. An AFTP can lead to both a considerable enrichment with carbon and oxygen and to the dilution of hydrogen. This depends on the envelope mass. The smaller envelope mass, the less hydrogen is left in the envelope (Blöcker 2001).

H-deficient central stars constitute at least 30% of all the central stars in the Galaxy (Weidmann & Gamen 2011). More than half of them are [WC] stars, which show emission line spectra typical for WR stars of carbon sequence (Acker & Neiner 2003). Hydrogen-deficient central stars are believed to expose their intershell region in their atmospheres due to a late helium-shell flash (Werner & Herwig 2006).

The evolution of post-AGB stars remains one of the most difficult topics in stellar evolution (Miller Bertolami 2019). The models must rely on assumptions and approximations such as mixing length theory or stellar wind theory. Observational verification is necessary for the validation of the evolutionary models.

Stellar luminosities and temperatures have been traditionally used to study the evolution of post-AGB stars. However, post-AGB stars occupy a narrow range in luminosities in the H-R diagram. Their distances are little known and the stars emit most of their energy in the ultraviolet range. Observational errors propagate large uncertainties in the determination of the luminosities.

An alternative set of parameters useful for studying the evolution of post-AGB stars is the stellar temperature and heating

[★] Reduced spectra are only available in electronic form at the CDS via anonymous ftp to cdsarc.u-strasbg.fr (130.79.128.5) or via <http://cdsweb.u-strasbg.fr/cgi-bin/qcat?J/A+A/>

Table 1. Log of the PNe observations.

Name	Exp. [s]	Date	Airmass	Other obs.
Jacoby LMC 17	2703	2013 Nov 08	1.33	[1],[2]
MGPN LMC 35	2845	2013 Nov 09	1.21	[2],[3]
MGPN LMC 39	2103	2013 Dec 22	1.26	[2],[3]
SMP LMC 26	2703	2013 Dec 21	1.29	[4]
SMP LMC 31	2785	2013 Nov 09	1.30	[2],[4],[5]
SMP LMC 55	2703	2013 Dec 22	1.29	[2],[4],[5]
SMP LMC 64	2103	2013 Nov 07	1.25	[2],[5],[6]
SMP LMC 67	2733	2013 Dec 23	1.24	[2],[5],[6],[7]
SMP LMC 104A	2703	2013 Nov 10	1.33	[7]
MGPN SMC 8	2703	2013 Nov 08	1.29	[3],[4],[8],[9]
SMP SMC 1	2103	2013 Nov 08	1.33	[1],[5],[9]
SMP SMC 12	2103	2013 Nov 07	1.36	[7],[9]
SMP SMC 16	2103	2013 Nov 09	1.35	[1],[3],[5],[6]
SMP SMC 28	2703	2013 Nov 10	1.35	[4],[6],[7]

References. [1] Boroson & Liebert (1989), [2] Reid & Parker (2006) [3] Vassiliadis et al. (1992), [4] Monk et al. (1988), [5] Meatheringham & Dopita (1991), [6] Shaw et al. (2006), [7] Leisy & Dennefeld (2006), [8] Shaw et al. (2010), [9] Stanghellini et al. (2003).

rate. The heating rate is a sensitive measure of the stellar mass. The pace of the temperature evolution is determined by the ratio of the stellar luminosity and remaining envelope mass.

Gesicki et al. (2014) derived heating rates from stellar temperatures and nebular ages for a sample of Galactic Bulge PNe. They needed to accelerate the evolutionary models by a factor of three to fit the white dwarf mass distribution and asteroseismological masses of central stars of PNe.

New models by Miller Bertolami (2016) confirmed the results obtained by Gesicki et al. (2014). He obtained three to ten shorter timescales of post-AGB evolution than Bloeker (1995) and Vassiliadis & Wood (1994). His models were also brighter by $\sim 0.1 - 0.3$ dex for the same mass. He took advantage of an updated treatment of the constitutive microphysics and included an updated description of the mixing processes and winds.

An alternative method to derive heating rate is to measure the temperature evolution of the central star. This could be derived indirectly by comparison of the nebular line fluxes in different epochs. The change of the $[\text{O III}]$ 5007 Å-to- $\text{H}\beta$ flux ratio in time is sensitive to the temperature evolution of cool central stars (Hajduk et al. 2015).

In this paper, we derived heating rates for a sample of central stars in the Magellanic Clouds and compared them with the existing evolutionary models. An advantage of Magellanic Cloud objects over Galactic PNe is the precisely determined distance. Moreover, Magellanic cloud PNe are often compact and spatially unresolved by ground based telescopes. In such cases, the ion stratification in the nebula would not affect the measured flux ratios.

2. Observations

We observed the fourteen PNe with the South African Large Telescope (SALT) equipped with the Robert Stobie Spectrograph (Kobulnicky et al. 2003; Burgh et al. 2003). The SALT telescope has a fixed azimuthal angle. The Magellanic Clouds were accessible with the SALT near the meridian (hour angle from -2 to 2), so that the observing track length was sufficiently long. Under these conditions, atmospheric refraction should not play a significant role.

Table 2. Log of the standard star observations.

Name	Exp. [s]	Date	Air mass
HILT 600	180	2013 Nov 07	1.23
HILT 600	180	2013 Nov 08	1.23
HILT 600	180	2013 Nov 09	1.22
EG 21	60	2013 Dec 22	1.24

Three chips recorded each spectrum in different wavelength ranges: 4345-5347 Å, 5403-6393 Å, and 6448-7397 Å. We used longslit with the projected width of two arcsec. The resulting resolution was about 800 in the center of the spectral range. The slit was oriented north-south. The range of air masses for the targets and standards was 1.21 – 1.36 (Tables 1 and 2). The log of observations is given in Table 1.

The spectra were extracted and wavelength calibrated. We calibrated the flux scale using a standard observed during the same night. On three nights: November 10, December 21, and December 22, flux standards were not observed. For these three nights we used the sensitivity curve derived for the closest night.

We measured the emission line fluxes with the Gaussian fit. We computed the errors of individual lines according to the formulae provided by Lenz & Ayres (1992). We added the derived error (root mean-square) of the sensitivity curve. We computed an error using at least two closest sensitivity curves if the standard was not observed during the given night. The fluxes were dereddened using the extinction law given by Fitzpatrick (1999) and the total to selective extinction ratio $R_V = 3.1$ (Table A.1). We derived the extinction from the observed $\text{H}\alpha$ -to- $\text{H}\beta$ line flux ratio.

3. New [WC] central stars

Hydrogen- and helium-burning post-AGB stars have different evolutionary tracks. Helium-burning tracks show slower evolution by approximately a factor of three in comparison to H-burning tracks for the same remnant mass.

In order to compare the evolution of the central stars of PNe with the evolutionary tracks, one needs to know which shell is active. This can be inferred from the photospheric abundances

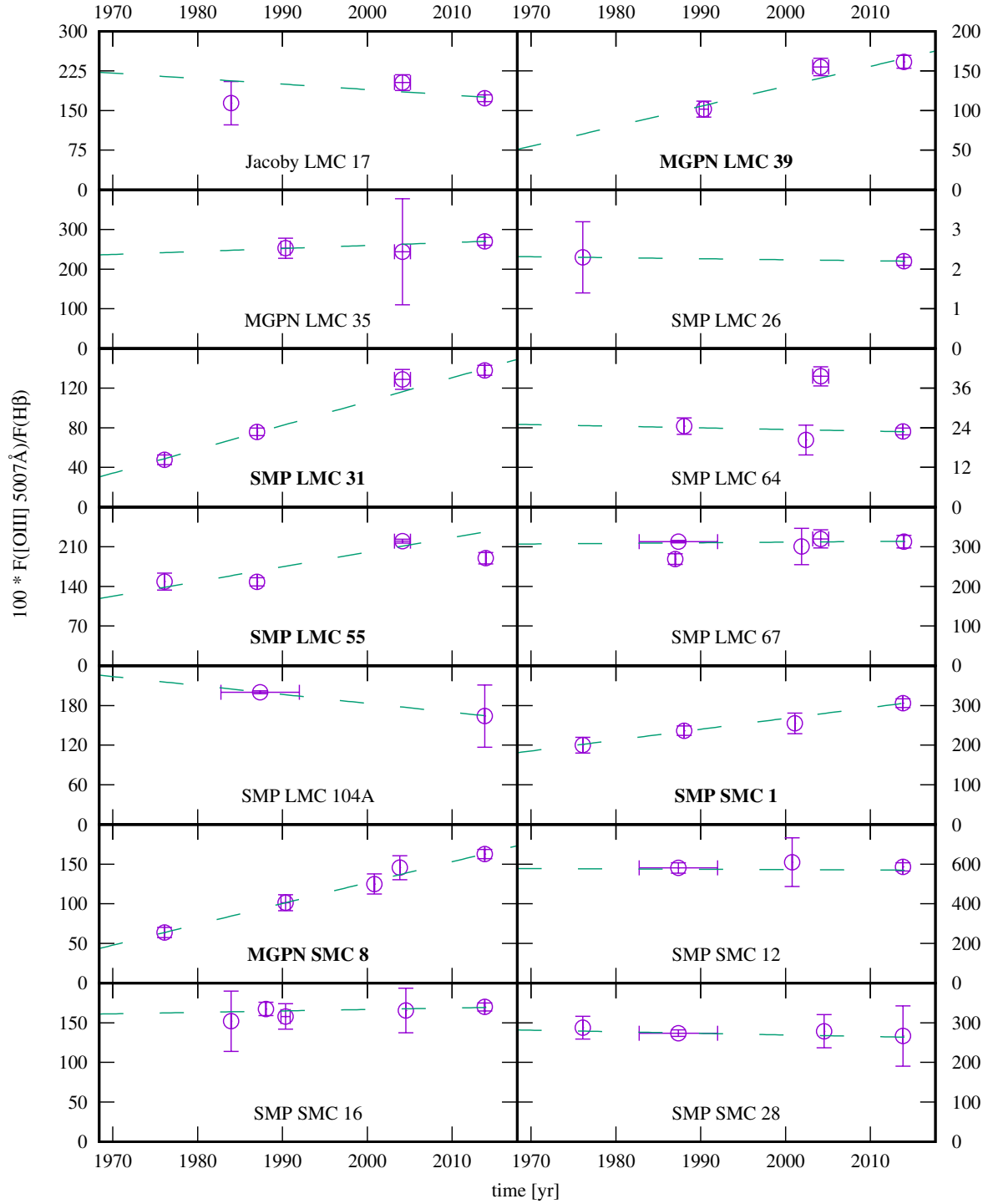


Fig. 1. Evolution of [O III] 5007 Å-to-H β line flux ratio in the Magellanic Cloud PNe. The dashed line fits the observed trend. The horizontal error bars correspond to the flux uncertainties. The vertical error bars in the time domain correspond to the observations, of which the dates were not precisely specified. Meatheringham & Dopita (1991) did not specify dates of their observations precisely, thus the error bars in time domain are large.

of a star. A hydrogen-poor atmosphere indicates that the star is a helium burner.

Most of the H-deficient central stars show [WC] spectra (Weidmann & Gamen 2011). They are relatively easy to identify, even if the stellar continuum is unobservable, since they show wide and prominent stellar wind lines imposed on the nebular spectrum (Acker & Neiner 2003). A hydrogen-rich atmosphere does not unambiguously indicate which shell is the main

source of the energy in the star. However, we assumed the stars that do not show emission lines to be H burners.

One of the stars in the sample (MGP SMC 8) is a known [WC] central star (Pena et al. 1997). We detected three more [WC] stars in our sample: SMPLMC 31, SMPLMC 55, and SMP SMC 1. They show emission lines of C III, C IV, and He II. The He II 4686 Å line in SMPLMC 31 has a full width at half maximum (FWHM) of 13 Å, while SMPLMC 55 and

SMP SMC 1 have FWHMs of C IV 4650 Å lines of 12 Å and 8 Å, respectively. Neither of the new [WC] stars show the C IV 5806 Å line. Thus, we classify them as [WC 11] type (Acker & Neiner 2003).

4. Heating rates

We combined new and archival spectra of PNe to study the temperature evolution of their central stars. We used the [O III] 5007 Å-to-H β line ratio. This ratio is sensitive to the changes of stellar temperature for cool central stars due to a much higher ionization potential of O⁺ than hydrogen. Both lines are relatively strong and located close to each other, so wavelength-dependent calibration errors are reduced.

We fit a linear function to the [O III] 5007 Å-to-H β line flux ratio observed in different epochs for each PN (Fig. 1). We discarded one point by Reid & Parker (2006) for SMP LMC 64 from the fitting, which exceeded all other points by a factor of two. The fit slope was larger than one, at least by 3σ in five PNe, indicating an increasing stellar temperature.

Among the PNe showing the flux evolution, one (MGP SMC 8) was observed five times, three PNe were observed four times, and one PN has three observations. The observations show a linear increase of the [O III] 5007 Å-to-H β flux ratio in time. An exception is SMP LMC 55. The third observation by Reid & Parker (2006) is significantly higher than the last one. However, the [O III] 5007 Å-to-H β flux ratio determined by Reid & Parker (2006) appears to be systematically higher than fluxes measured by other authors.

We performed spherically symmetric photoionization models of these five PNe with the Cloudy v. 17.01 code. All the models were constrained by the observed absolute H β flux. We fit the nebular line flux ratios observed in 2013 (Table A.1).

The nebular sizes and stellar luminosities are available for three objects observed with the Hubble Space Telescope by Villaver et al. (2003) and Villaver et al. (2004). However, for the PN MGP SMC 8 temperature and luminosity, determination is most likely affected by the stellar contribution to the He II 4686 Å line flux (Shaw et al. 2010). For this and two other PNe, stellar luminosity was a free parameter. The adopted luminosities, or those derived from our photoionization models L_* , are given in Table 3.

We varied stellar temperature to obtain the best fit. We used atmosphere models by Castelli & Kurucz (2003). The grid covers the temperature range of 3.5 – 50 kK.

We used nebular abundances by Leisy & Dennefeld (2006) as an input parameter, but varied it to better fit the observed emission line fluxes. For some cases (e.g., MGP LMC 39, SMP LMC 31, and SMP SMC 1) we were not able to achieve the observed [O III] 5007 Å-to-H β line flux ratio with the O/H abundances derived by Leisy & Dennefeld (2006). At low metallicities, the [O III] 5007 Å-to-H β line flux ratio depends on the nebular O/H abundance and stellar temperature (Stasińska 2007). For the average SMC oxygen abundance, the [O III] 5007 Å-to-H β flux ratio reaches a maximum of five at a temperature of about 100 kK (Stanghellini et al. 2003). For the LMC, the models reach maximum of ten at similar stellar temperatures.

Table 3 shows the input parameters and results of the photoionization modeling of the five objects. The modeled line fluxes are compared to the fluxes measured in 2013 in Table A.2.

We varied stellar temperature to fit the [O III] 5007 Å-to-H β line flux ratio observed in other epochs. After we obtained the

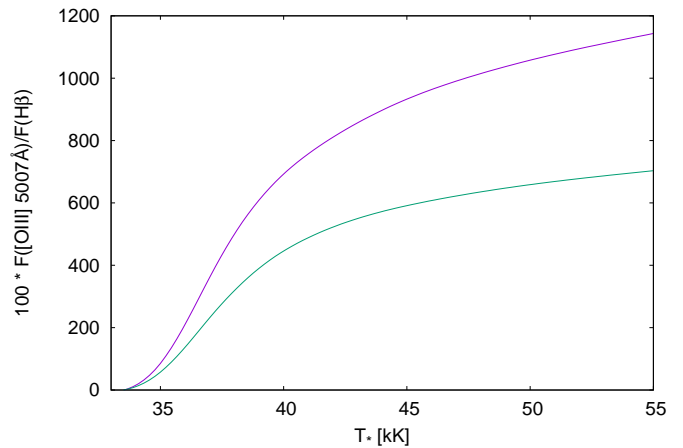


Fig. 2. Two models of the evolution of the [O III] 5007 Å-to-H β flux ratio with the temperature of the central star in a PN. The model parameters are identical to MGP LMC 39, and the second model the (O/H) abundance is lowered by 0.3 in dex.

temperatures in different years, we used them to compute heating rates \dot{T}_* . The uncertainty of the measured [O III] 5007 Å-to-H β line flux ratio propagates to the measured temperatures in different epochs and subsequently to the heating rates presented in Table 3.

We computed heating rates from the evolutionary tracks as a function of stellar temperature. We used models by Miller Bertolami (2016) for the star that does not show emission lines, and Vassiliadis & Wood (1994) for four [WC] central stars. Miller Bertolami (2016) computed only three He-burning models spanning a very low range of masses.

Heating rates derived from the evolutionary tracks were interpolated to fit observed heating rates. We determined model-dependent luminosities L_{MOD} and corresponding model-dependent masses M_{MOD} . The errors of L_{MOD} and M_{MOD} shown in Table 3 result from the uncertainties in \dot{T}_* .

We did not include systematic errors in measured heating rates in Table 3. These depend mostly on the determination of the O/H abundance. For an adopted uncertainty of the log (O/H) of 0.3 in dex, the model-dependent stellar mass M_{MOD} is accurate to about $0.04 M_{\odot}$, and log of luminosity to 0.15 dex. Moreover, the model-dependent masses for [WC] stars derived using tracks by Vassiliadis & Wood (1994) may be overestimated by $0.038 M_{\odot}$ (Gesicki et al. 2014).

Heating rates derived from the evolutionary tracks do not vary strongly with stellar temperature. The uncertainty of stellar temperature determination affects the derived model-dependent parameters to a much lower extent than the uncertainty in the determination of O/H abundance.

5. Discussion

We attempted to select PNe with relatively cool central stars to study their evolution. Our sample fulfils the criterion of [O III] 5007 Å-to-H β ratio ≤ 3 for all but one object. However, this criterion appeared to be insufficient in some cases. The [O III] 5007 Å line may be weak in hot PNe, due to photoionization of O⁺⁺ to O⁺⁺⁺ (Marigo et al. 2001; Stasińska 1989). Also, the [O III] 5007 Å line can be weak in PNe with low O abundances, despite a high temperature. This appears to be the case for three PNe in our sample: Jacoby LMC 17, MGP LMC 35,

Table 3. Input parameters and results of the photoionization modeling. Derived stellar temperatures, heating rates, model-dependent luminosities and masses for the central stars, modeled O and N abundances of the PNe, observed luminosities, temperatures, H β fluxes, and diameters.

Name	MGP N LMC 39 ^a	SMPLMC 31	SMPLMC 55	MGP N SMC 8	SMP SMC 1
T_* [kK]	35.7	34.8	37.3	37.3	37.2
\dot{T}_* [K yr ⁻¹]	19.1 \pm 4.7	18.4 \pm 1.5	10.4 \pm 2.1	24.9 \pm 2.4	17.8 \pm 3.4
log L_{MOD}/L_{\odot}	3.759 \pm 0.014	3.791 \pm 0.018	3.650 \pm 0.074	3.867 \pm 0.029	3.784 \pm 0.040
M_{MOD}/M_{\odot}	0.570 \pm 0.004	0.668 \pm 0.024	0.613 \pm 0.014	0.693 \pm 0.016	0.644 \pm 0.023
log(O/H)	-3.50	-3.92	-3.83	-3.65	-3.81
log(N/H)			-4.53		-4.62
log L_*/L_{\odot}	3.50 [1]	4.01 [2]	4.21 [1]	3.42 [1]	3.77 [3]
log T_* (H I) ^b		28.6 \pm 2.4 [2]		28.8 \pm 2.6 [3]	28.8 \pm 2.6 [3]
log $F(\text{H}\beta)$	-13.07 [4]	-12.91 [5]	-12.20 [4]	-13.27 [6]	-12.85 [6]
d [arcsec]		0.26 [5]		0.615 [6]	0.15 [6]

References. [1] this paper, [2] Villaver et al. (2003), [3] Villaver et al. (2004), [4] Reid & Parker (2006), [5] Stanghellini et al. (2002), [6] Stanghellini et al. (2003), ^acentral star without emission lines ^bcomputed using black-body model

and SMP SMC 28, which show prominent He II 4686 Å lines. These PNe are not expected to show rapid evolution of the [O III] 5007 Å flux.

Young PNe can mimic symbiotic stars due to high nebular density and strong dust emission. Ikiewicz & Mikołajewska (2017) listed two PNe from our sample, SMPLMC 31 and SMPLMC 104A, as symbiotic star candidates. However, we did not find any indication of the cool giant in their spectra. In addition, SMPLMC 31 show stellar wind lines consistent with a [WC] star.

Eleven out of fourteen PNe in our sample may be considered as young PNe. Five of them show an evolution of the [O III] 5007 Å line flux. The five central stars showing temperature evolution are most likely the most massive in our sample, and thus the most luminous. An independent luminosity determination confirms that these stars show the highest luminosities (Table 4).

The remaining six central stars may evolve too slowly to show significant evolution of the [O III] 5007 Å- to-H β flux ratio on a timescale of decades. The collected observations are sensitive down to heating rates of about 5 – 10 K yr⁻¹. Lower heating rates, corresponding to the initial masses below 1.25 M_{\odot} (final masses below 0.532 M_{\odot}) (Miller Bertolami 2019), would not be detected.

Figure 2 shows the modeled evolution of nebular [O III] 5007 Å- to-H β flux ratio with increasing stellar temperature for two different O/H abundance ratios. The [O III] 5007 Å- to-H β flux ratio scales approximately with the O abundance. The flux ratio does not increase linearly throughout the whole temperature range of the central star, but it can be approximated as linear in sufficiently small temperature intervals. The heating rate is highest between 35 and 38 kK. Then it slows down. The five central stars of which the nebulae show flux evolution have stellar temperatures in this range.

The central star of MGP N LMC 39 is probably the most massive H-burning central star in our sample. Its final mass of 0.57 M_{\odot} is the same as the peak of the mass distribution for the central stars of Galactic PNe. The remaining H-burning central stars in our sample are less massive. This suggests that central stars in the Magellanic Clouds are less massive than the stars in the Galaxy. Hajduk et al. (2014) derived heating rates of 45 ± 7 K yr⁻¹ for Galactic PN Hen 2-260, significantly higher than for Magellanic Cloud central stars.

We compared the model-dependent luminosities L_{MOD} with luminosities determined independently using different methods: using Zanstra temperatures and a black-body fit (log T_* (H I)), by fitting spectral energy distribution (SED) (L_{SED}) and by photoionization modeling (L_*) (Tab. 4). Unfortunately, the luminosities yielded from observations using different methods show a relatively large scatter.

The model-dependent luminosity agrees with the observed luminosity for SMP SMC 1 and is within the observed range of stellar luminosities for other objects. For SMPLMC 55, the model-dependent luminosity is close to the luminosity derived from photoionization modeling by Dopita & Meatheringham (1991), but lower by 0.56 dex from the luminosity of our photoionization model. However, the absolute H β flux used by Dopita & Meatheringham (1991) was 0.46 lower in log than that used by us from Reid & Parker (2006). If this discrepancy were real, this would indicate an unexpected change in luminosity of this object.

We are not able to discriminate between Miller Bertolami (2016) and Vassiliadis & Wood (1994) or Bloeker (1995). Miller Bertolami (2016) models were faster and more luminous for the same masses. However, these models all show similar evolutionary speeds for the same luminosity of the central star (but different masses). We would be able to discriminate between these models if we obtained an independent mass determination.

The [WC] central stars constitute about 15% of Galactic central stars of PNe. This ratio was suggested to be as low as 5% in the Magellanic Clouds (Pena et al. 1997). Pena et al. (1997) reported only two [WC] central stars in the Small Magellanic Cloud (SMC) and six in the Large Magellanic Cloud (LMC). Five stars are intermediate types [WC 4] or [WC 4-5], and only one is [WC 9] (Monk et al. 1988). Margon et al. (2020a) and Margon et al. (2020b) announced the discovery of two more [WC 11] stars in the LMC. They suggested that a large population of late-type [WC] stars may exist, undetected due to observational selection. Late-type [WC] stars show faint emission lines, which could be missed in observations performed with smaller telescopes. We discovered three new late-type [WC] stars.

Interestingly, the four [WC] PNe observed by us show rapid evolution. This implies relatively high stellar mass. Hajduk et al. (2015) observed a relatively rapid change of the [O III] 5007 Å- to-H β flux ratio for the Galactic PNe M 1-11 and M 1-12 contain-

Table 4. Luminosities of the central stars of PNe obtained using different methods: model-dependent luminosities determined from heating rates, luminosities derived from Zanstra temperatures and stellar magnitudes, from the integrated spectral energy distribution, and constrained from absolute H β flux and nebular modeling. For SMP LMC 64 and SMP LMC 104A, no data were found in the literature.

ref.	$\log L_{\text{MOD}}$ [1]	$\log L_*/L_\odot$ (H I) [2]	$\log L_{\text{SED}}/L_\odot$ [3]	$\log L_{\text{SED}}/L_\odot$ [4]	$\log L_*/L_\odot$ [5]	$\log L_*/L_\odot$ [1]
Jacoby LMC 17			3.39			
MGPn LMC 35			3.20			
MGPn LMC 39	3.759		3.70	3.47		3.50
SMP LMC 26			3.60	3.32		
SMP LMC 31	3.791	4.01	3.90	3.64		
SMP LMC 55	3.650				3.69	4.21
SMP LMC 67				2.86	3.33	
MGPn SMC 8	3.867	4.33		3.49		3.42
SMP SMC 1	3.784	3.77				
SMP SMC 12		2.84				
SMP SMC 16				3.20		
SMP SMC 28					3.28	

References. [1] this paper, [2] Villaver et al. (2003, 2004), [3] van Aarle et al. (2011), [4] Kamath et al. (2014), [5] Dopita & Meatheringham (1991)

ing [WC] central stars. This suggests that the evolution of Galactic [WC] stars also is faster than H-rich central stars and originate from more massive progenitors. This was independently confirmed by Weidmann & Gamen (2011), who found that H-poor central stars are more concentrated toward the Galactic center and Galactic plane than the H-rich group. The DB white dwarfs, which are the possible progeny of [WC] central stars, show an average mass of $0.651 M_\odot$, higher than the $0.598 M_\odot$ derived for DA white dwarfs, which originate from H-rich central stars (Kleinman et al. 2013).

Acknowledgements. MH thanks the Ministry of Science and Higher Education (MSHE) of the Republic of Poland for granting funds for the Polish contribution to the International LOFAR Telescope (MSHE decision no. DIR/WK/2016/2017/05-1) and for maintenance of the LOFAR PL-612 Baldy (MSHE decision no. 59/E-383/SPUB/SP/2019.1). Polish participation in SALT is funded by the MSHE grant No. DIR/WK/2016/07. MH acknowledges financial support from National Science Centre, Poland, grant No. 2016/23/B/ST9/01653. Some of the observations reported in this paper were obtained with the Southern African Large Telescope (SALT) under programme 2013-2-POL_OTH-001 (PI M. Hajduk).

References

Acker, A. & Neiner, C. 2003, A&A, 403, 659
 Blöcker, T. 2001, Ap&SS, 275, 1
 Bloeker, T. 1995, A&A, 299, 755
 Boroson, T. A. & Liebert, J. 1989, ApJ, 339, 844
 Burgh, E. B., Nordsieck, K. H., Kobulnicky, H. A., et al. 2003, Society of Photo-Optical Instrumentation Engineers (SPIE) Conference Series, Vol. 4841, Prime focus imaging spectrograph for the Southern African large telescope: optical design, ed. M. Iye & A. F. M. Moorwood, 1463–1471
 Castelli, F. & Kurucz, R. L. 2003, in IAU Symposium, Vol. 210, Modelling of Stellar Atmospheres, ed. N. Piskunov, W. W. Weiss, & D. F. Gray, A20
 Dopita, M. A. & Meatheringham, S. J. 1991, ApJ, 367, 115
 Fitzpatrick, E. L. 1999, PASP, 111, 63
 Gesicki, K., Zijlstra, A. A., Hajduk, M., & Szyszka, C. 2014, A&A, 566, A48
 Hajduk, M., van Hoof, P. A. M., Gesicki, K., et al. 2014, A&A, 567, A15
 Hajduk, M., van Hoof, P. A. M., & Zijlstra, A. A. 2015, A&A, 573, A65
 Herwig, F. 2005, ARA&A, 43, 435
 Iben, I., J. & Renzini, A. 1983, ARA&A, 21, 271
 Ilkiewicz, K. & Mikołajewska, J. 2017, A&A, 606, A110
 Kamath, D., Wood, P. R., & Van Winckel, H. 2014, MNRAS, 439, 2211
 Karakas, A. I. 2010, MNRAS, 403, 1413
 Kleinman, S. J., Kepler, S. O., Koester, D., et al. 2013, ApJS, 204, 5

Kobulnicky, H. A., Nordsieck, K. H., Burgh, E. B., et al. 2003, Society of Photo-Optical Instrumentation Engineers (SPIE) Conference Series, Vol. 4841, Prime focus imaging spectrograph for the Southern African large telescope: operational modes, ed. M. Iye & A. F. M. Moorwood, 1634–1644
 Koesterke, L. 2001, Ap&SS, 275, 41
 Leisy, P. & Dennefeld, M. 2006, A&A, 456, 451
 Lenz, D. D. & Ayres, T. R. 1992, PASP, 104, 1104
 Margon, B., Manea, C., Williams, R., et al. 2020a, ApJ, 888, 54
 Margon, B., Massey, P., Neugent, K. F., & Morrell, N. 2020b, arXiv e-prints, arXiv:2006.04333
 Marigo, P., Girardi, L., Groenewegen, M. A. T., & Weiss, A. 2001, A&A, 378, 958
 Meatheringham, S. J. & Dopita, M. A. 1991, ApJS, 75, 407
 Miller Bertolami, M. M. 2016, A&A, 588, A25
 Miller Bertolami, M. M. 2019, in IAU Symposium, Vol. 343, IAU Symposium, ed. F. Kerschbaum, M. Groenewegen, & H. Olofsson, 36–46
 Monk, D. J., Barlow, M. J., & Clegg, R. E. S. 1988, MNRAS, 234, 583
 Paczyński, B. 1970, Acta Astron., 20, 47
 Pena, M., Ruiz, M. T., & Torres-Peimbert, S. 1997, A&A, 324, 674
 Reid, W. A. & Parker, Q. A. 2006, MNRAS, 373, 521
 Schoenberger, D. 1979, A&A, 79, 108
 Shaw, R. A., Lee, T.-H., Stanghellini, L., et al. 2010, ApJ, 717, 562
 Shaw, R. A., Stanghellini, L., Villaver, E., & Mutchler, M. 2006, ApJS, 167, 201
 Stanghellini, L., Shaw, R. A., Balick, B., et al. 2003, ApJ, 596, 997
 Stanghellini, L., Shaw, R. A., Mutchler, M., et al. 2002, ApJ, 575, 178
 Stasińska, G. 1989, A&A, 213, 274
 Stasińska, G. 2007, arXiv e-prints, arXiv:0704.0348
 van Aarle, E., van Winckel, H., Lloyd Evans, T., et al. 2011, A&A, 530, A90
 Vassiliadis, E., Dopita, M. A., Morgan, D. H., & Bell, J. F. 1992, ApJS, 83, 87
 Vassiliadis, E. & Wood, P. R. 1994, ApJS, 92, 125
 Villaver, E., Stanghellini, L., & Shaw, R. A. 2003, ApJ, 597, 298
 Villaver, E., Stanghellini, L., & Shaw, R. A. 2004, ApJ, 614, 716
 Weidmann, W. A. & Gamen, R. 2011, A&A, 526, A6
 Werner, K. & Herwig, F. 2006, PASP, 118, 183

Appendix A: Line fluxes

Table A.1. The measured and dereddened line fluxes in the LMC PNe with the relevant uncertainties. The value of the $E(B - V)$ color excess applied for dereddening the fluxes is given for each PN.

	λ	Jacoby LMC 17			MGPN LMC 35			MGPN LMC 39			SMPLMC 26			SMPLMC 31		
		$F(\lambda)$	$I(\lambda)$	δI	$F(\lambda)$	$I(\lambda)$	δI	$F(\lambda)$	$I(\lambda)$	δI	$F(\lambda)$	$I(\lambda)$	δI	$F(\lambda)$	$I(\lambda)$	δI
$E(B - V)$			0.36			0.10			0.45			0.19			0.37	
H γ	4343	38.6	45.5	1.7	43.7	45.8	3.4							43.2	51.1	1.9
[O III]	4363	20.6	24.1	1.0	30.1	31.5	3.3							0.9	1.1	0.2
He I	4388													0.4	0.5	0.1
He I	4471							2.6	3.1	0.4				2.8	3.2	0.2
He II	4541	2.0	2.2	0.3										1.5	1.6	0.2
C IV	4650							1.4 ^a	1.6 ^a	0.3 ^a				1.5 ^a	1.6 ^a	0.2 ^a
He II	4686	10.2	10.8	0.6	58.3	59.2	2.7									
[Ar IV]/He I	4712	1.0	1.1	0.2										0.5	0.5	0.1
[Ne IV]	4726	1.4	1.4	0.3												
[Ar IV]	4741	0.7	0.7	0.2												
H β	4861	100.0	100.0	3.6	100.0	100.0	4.0	100.0	100.0	5.0	100.0	100.0	5.0	100.0	100.0	3.6
He I	4922													0.9	0.9	0.1
[O III]	4931															
[O III]	4959	65.1	63.0	2.3	88.5	87.7	3.5	54.7	52.5	2.7	0.5	0.5	0.1	48.7	47.1	1.7
[O III]	5007	182.0	173.4	6.2	274.2	270.5	9.9	170.0	160.1	8.0	2.3	2.2	0.1	145.6	138.6	5.0
[N I]	5197										0.6	0.6	0.1	0.3	0.3	0.1
He II	5412	6.2	5.2	0.2	6.4	6.1	0.8									
[Cl III]	5537													0.1	0.1	0.1
C III	5696													0.8 ^a	0.6 ^a	0.1 ^a
[N II]	5755	4.1	3.2	0.2				2.2	1.6	0.2	2.7	2.4	0.1	3.6	2.8	0.2
He I	5876	5.3	4.0	0.2	10.9	10.1	1.0	12.4	8.7	0.5	1.8	1.5	0.1	13.7	10.3	0.4
[O I]	6302	13.2	9.1	0.3	5.2	4.7	0.5	2.6	1.6	0.2	2.3	1.9	0.1	3.3	2.2	0.1
[S III]	6312	2.7	1.9	0.1				2.1	1.3	0.1				1.0	0.7	0.1
[O I]	6347													0.3	0.2	0.1
[O I]	6365	4.7	3.2	0.1	3.9	3.5	0.7	0.7	0.4	0.1	0.5	0.5	0.1	1.2	0.8	0.1
[N II]	6548	15.2	10.0	0.4	14.1	12.5	0.7	15.7	9.3	0.5	41.6	33.6	1.7	23.6	15.5	0.6
H α	6563	433.5	286.0	10.1	321.9	286.0	10.2	482.6	286.0	14.2	355.0	286.0	14.2	438.5	286.0	10.2
[N II]	6584	34.5	22.7	0.8	28.3	25.1	1.1	42.9	25.3	1.3	119.0	95.7	4.7	71.7	46.6	1.7
He I	6678	1.7	1.1	0.1	2.9	2.6	0.5	3.9	2.3	0.2	0.6	0.5	0.9	4.3	2.8	0.2
[S II]	6716	2.0	1.3	0.1	4.8	4.2	0.6	3.9	0.6	0.1	0.4	0.3	0.1	0.5	0.3	0.1
[S II]	6730	2.4	1.5	0.1	4.5	4.0	0.5				1.7	1.4	0.1	1.1	0.7	0.1
He I	7002															
[Ar V]	7007	3.1	1.9	0.1	4.0	3.5	0.5	11.4	6.1	0.4	0.4	0.3	0.1			
He I	7065	3.3	2.0	0.1	7.3	6.4	0.6				0.8	0.6	0.1			
[Ar III]	7100							11.2	5.9	0.3				0.5	0.3	0.1
[Ar III]	7136	7.2	4.3	0.2	7.4	6.4	0.7				1.0	0.8	0.1	9.2	5.4	0.2
[Ar IV]	7172	1.5	0.9	0.1				2.4	1.3	0.1						
[Ar IV]	7237													2.0	1.2	0.1
He I	7281							1.0	0.5	0.1				1.1	0.6	0.1
[O II]	7320	8.5	5.0	0.2				65.9	33.5	1.7	23.4	17.7	0.9	46.2	26.6	1.0
[O II]	7330	6.9	4.0	0.2				49.0	24.9	1.3	17.6	13.3	0.7	36.8	21.1	0.8

^a stellar line

Table A.1. The measured and dereddened line fluxes in the MC PNe with the relevant uncertainties. The value of the $E(B - V)$ color excess applied for dereddening the fluxes is given for each PN.

	λ	SMPLMC 55			SMPLMC 64			SMPLMC 67			SMPLMC 104A			MGPN SMC 8		
		$F(\lambda)$	$I(\lambda)$	δI	$F(\lambda)$	$I(\lambda)$	δI	$F(\lambda)$	$I(\lambda)$	δI	$F(\lambda)$	$I(\lambda)$	δI	$F(\lambda)$	$I(\lambda)$	δI
$E(B - V)$			0.25			0.52			0.22			0.23			0.26	
H γ	4343				56.5	71.8	1.9				51.0	56.7	16.1	35.1	39.5	1.5
[O III]	4363	1.3	1.5	0.2	3.2	4.1	0.2	1.4	1.6	0.2	21.1	23.2	6.6	2.3	2.6	0.3
He I	4388	0.5	0.6	0.1	1.0	1.3	0.2	0.6	0.6	0.1	0.2	0.2	0.1			
He I	4471	3.4	3.7	0.2	4.4	5.3	0.2	4.3	4.5	0.3	1.5	1.5	0.5	4.4	4.8	0.3
He II	4541	0.4	0.4	0.1	1.4	1.6	0.1				2.2	2.3	0.7	1.9	2.0	0.2
C IV	4650	1.1 ^a	1.1 ^a	0.1 ^a										119.5 ^a	125.6 ^a	4.5 ^a
He II	4686	1.1 ^a	1.1 ^a	0.1 ^a							62.2	65.0	18.4	24.9 ^a	26.0 ^a	1.0 ^a
[Ar IV]/He I	4712	0.5	0.6	0.1	0.5	0.6	0.1	0.6	0.6	0.1	1.5	1.5	0.5			
[Ne IV]	4726										1.5	1.5	0.5			
[Ar IV]	4741										1.1	1.1	0.4			
H β	4861	100.0	100.0	5.0	100.0	100.0	2.6	100.0	100.0	5.0	100.0	100.0	28.3	100.0	100.0	3.6
He I	4922	0.9	0.8	0.1	2.4	2.3	0.1	1.3	1.3	0.1	0.6	0.6	0.2	1.0	1.0	0.2
[O III]	4931										0.5	0.5	0.2			
[O III]	4959	64.4	62.9	3.2	6.3	6.1	0.2	105.1	103.4	5.2	56.8	54.4	15.4	53.7	52.5	1.9
[O III]	5007	193.8	187.3	9.3	22.8	21.3	0.6	320.4	303.7	15.1	172.1	163.8	46.4	168.2	162.5	5.8
[N I]	5197	0.5	0.4	0.1	1.3	1.1	0.1	1.4	1.4	0.1						
He II	5412															
[Cl III]	5537	0.2	0.2	0.1				0.3	0.2	0.1						
C III	5696	0.4 ^a	0.3 ^a	0.1 ^a										51.1 ^a	43.0 ^a	1.5 ^a
[N II]	5755	2.3	1.9	0.1				4.1	3.5	0.2	0.7	0.6	0.2			
He I	5876	13.3	10.9	0.6				16.0	12.9	0.7	5.0	4.2	1.2			
[O I]	6302	2.8	2.2	0.2	6.4	3.8	0.1	2.1	1.7	0.1	2.9	2.3	0.7	6.8	5.2	0.2
[S III]	6312	1.2	0.9	0.1	5.1	3.0	0.1	0.7	0.6	0.1	1.6	1.2	0.4	1.1	0.9	0.1
[O I]	6347															
[O I]	6365	0.9	0.7	0.1	2.1	1.2	0.1	0.7	0.6	0.1	0.9	0.7	0.3	2.3	1.7	0.1
[N II]	6548	34.0	25.4	1.3	37.4	20.5	0.6	102.3	80.4	4.0	5.3	4.1	1.2	37.1	27.6	1.0
H α	6563	384.3	286.0	14.2	522.8	286.0	7.2	364.8	286.0	14.2	372.3	286.0	80.9	385.8	286.0	10.2
[N II]	6584	102.3	75.9	3.8	50.3	27.3	0.7	309.6	240.3	11.9	3.0	2.3	0.7	116.3	86.0	3.1
He I	6678	4.0	2.9	0.2	2.7	1.4	0.1	4.7	3.7	0.2	0.9	0.7	0.2	0.9	0.7	0.1
[S II]	6716	1.7	1.2	0.1	0.6	0.3	0.1	3.4	2.6	0.2	0.3	0.2	0.1	10.7	7.8	0.3
[S II]	6730	3.4	2.4	0.2	0.9	0.5	0.1	5.0	3.8	0.2	0.5	0.3	0.1	14.4	10.5	0.4
He I	7002	0.2	0.1	0.3	0.5	0.2	0.1	0.1	0.1	0.1						
[Ar V]	7007										2.3	1.7	0.5			
He I	7065	9.9	6.9	2.3	4.6	2.2	0.1	6.2	4.6	0.3	3.8	2.8	0.8	6.7	4.7	0.2
[Ar III]	7100															
[Ar III]	7136	28.7	6.3	2.1	5.7	2.7	0.1	9.2	6.7	0.4	3.1	2.2	0.7	6.6	4.6	0.2
[Ar IV]	7172	21.8	0.7	0.5	0.4	0.2	0.1				0.6	0.5	0.2			
[Ar IV]	7237															
He I	7281	1.0	0.7	0.5	0.7	0.3	0.1	0.9	0.7	0.1	0.3	0.2	0.1			
[O II]	7320	28.7	19.6	6.0	24.5	11.2	0.3	7.1	5.2	0.3	3.8	2.8	0.8	16.0	10.8	0.4
[O II]	7330	21.8	14.9	4.8	19.2	8.8	0.3	6.0	4.4	0.3	3.1	2.2	0.7	12.0	8.2	0.3

^a stellar line

Table A.1. The measured and dereddened line fluxes in the SMC PNe with the relevant uncertainties. The value of the $E(B - V)$ color excess applied for dereddening the fluxes is given for each PN.

	λ	SMP SMC 1			SMP SMC 12			SMP SMC 16			SMP SMC 28		
		$F(\lambda)$	$I(\lambda)$	δI	$F(\lambda)$	$I(\lambda)$	δI	$F(\lambda)$	$I(\lambda)$	δI	$F(\lambda)$	$I(\lambda)$	δI
$E(B - V)$			0.03			0.00			0.13			0.06	
H γ	4343				54.0	54.0	2.3	37.9	40.6	1.3	41.9	43.1	12.2
[O III]	4363	2.4	2.4	0.2	8.4	8.4	0.9				12.3	12.6	3.6
He I	4388	0.6	0.6	0.1									
He I	4471	4.6	4.7	0.2	3.0	3.0	0.5	3.3	3.5	0.2	6.1	6.3	1.8
He II	4541										1.9	1.9	0.6
C IV	4650	2.0 ^a	2.0 ^a	0.2 ^a							1.3	1.3	0.4
He II	4686	0.4	0.4	0.1							58.4	59.0	16.7
[Ar IV]/He I	4712	0.7	0.8	0.1	1.6	1.6	0.4	0.8	0.8	0.2	5.3	5.4	1.6
[Ne IV]	4726										1.5	1.5	0.5
[Ar IV]	4741										4.9	4.9	1.4
H β	4861	100.0	100.0	3.6	100.0	100.0	3.7	100.0	101.1	2.9	100.0	100.0	28.3
He I	4922	0.8	0.8	0.1	0.6	0.6	0.3	1.0	1.0	0.1	1.4	1.4	0.4
[O III]	4931												
[O III]	4959	101.5	101.3	3.6	197.2	197.2	7.1	57.7	57.7	1.7	89.8	89.3	25.3
[O III]	5007	304.5	303.4	10.8	591.5	591.5	21.1	171.7	170.7	4.9	267.4	265.3	75.1
[N I]	5197										2.2	2.1	0.7
He II	5412										3.9	3.8	1.1
[Cl III]	5537							0.2	0.1	0.1			
C III	5696	0.3 ^a	0.3 ^a	0.1 ^a									
[N II]	5755	1.1	1.1	0.1				0.8	0.7	0.1	8.5	8.1	2.4
He I	5876	14.1	13.8	0.5	14.6	14.6	0.6	12.7	11.7	0.4			
[O I]	6302	1.8	1.8	0.1				1.6	1.4	0.1	3.1	2.9	0.9
[S III]	6312	0.7	0.7	0.1				0.5	0.5	0.1	2.9	2.7	0.8
[O I]	6347	0.1	0.1	0.1									
[O I]	6365	0.6	0.6	0.1				0.6	0.6	0.1	0.9	0.9	0.3
[N II]	6548	8.4	8.2	0.3				14.3	12.5	0.4	62.1	58.0	16.4
H α	6563	295.5	286.0	10.2	270.4	270.4	9.6	327.2	286.0	8.1	306.5	286.0	80.9
[N II]	6584	22.9	22.1	0.8	1.4	1.4	0.2	41.3	36.0	1.1	174.2	162.4	46.0
He I	6678	3.6	3.5	0.2	3.7	3.7	0.2	3.6	3.1	0.1	4.9	4.5	1.3
[S II]	6716	0.3	0.3	0.1				1.3	1.1	0.1	3.9	3.6	1.1
[S II]	6730	0.6	0.6	0.1				2.5	2.1	0.1	6.8	6.3	1.8
He I	7002	0.2	0.2	0.1									
[Ar V]	7007										2.2	2.0	0.6
He I	7065	10.3	9.9	0.4	3.9	3.9	0.3	8.2	7.0	0.3	12.5	11.5	3.3
[Ar III]	7100	0.3	0.3	0.1									
[Ar III]	7136	5.2	5.0	0.2	1.9	1.9	0.2	3.4	2.8	0.1	9.1	8.4	2.4
[Ar IV]	7172										1.4	1.3	0.4
[Ar IV]	7237	1.7	1.6	0.1				0.8	0.7	0.1			
He I	7281	1.0	1.0	0.1				1.0	0.9	0.1	1.3	1.2	0.4
[O II]	7320	16.4	15.7	0.6				13.2	11.1	0.4	4.2	3.8	1.1
[O II]	7330	13.3	12.7	0.5				10.2	8.5	0.3	3.4	3.1	0.9

^a stellar line

Table A.2. The modeled and observed line-flux ratios in the five MC PNe showing the evolution of the [O III] 5007 Å line flux.

ID	λ	MGPN LMC 39		SMP LMC 31		SMP LMC 55		MGPN SMC 8		SMP SMC 1	
		Model	Observed	Model	Observed	Model	Observed	Model	Observed	Model	Observed
[O III]	4363			0.8	1.1	1.4	1.5	1.3	2.6	2.5	2.4
He I	4471	2.1	3.1	1.7	3.2	2.9	3.7	2.7	4.8	3.4	4.7
He I	4713		0.6	0.2	0.5	0.4	0.6			0.5	0.8
H β	4861	100.0	100.0	100.0	100.0	100.0	100	100.0	100.0	100.0	100.0
He I	4922			0.5	0.9	0.8	0.8	0.7	1.0	0.9	0.8
[O III]	4959	47.9	52.5	42.0	47.1	58.7	62.9	63.5	52.5	99.2	101.5
[O III]	5006	143.0	160.1	125.4	138.6	175.1	187.3	189.6	162.5	296.0	303.4
[N I]	5197			0.0	0.3	1.8	0.4				
[N II]	5755	1.0	1.6	0.6	2.8	8.4	1.9			1.9	1.1
He I	5876	6.0	8.7	4.3	10.3						
[O I]	6300	3.8	1.6	1.6	2.2	3.1	2.2	4.2	5.2	2.9	1.8
[S III]	6312	2.8	1.3	0.6	0.7	0.7	0.9	0.7	0.9	0.2	0.7
[O I]	6363	1.2	0.4	0.5	0.8	1.0	0.7	1.3	1.7	0.9	0.6
[N II]	6548	8.0	9.3	12.5	15.5	19.9	25.4	30.2	27.6	24.1	8.2
H α	6563	277.8	286.0	277.2	286.0	277.4	286.0	278.3	286.0	277.7	286.0
[N II]	6584	23.7	25.3	36.8	46.6	58.8	75.9	88.9	86.0	71.0	22.1
He I	6678	1.6	2.3	1.3	2.8	2.2	2.9	2.0	0.7	2.6	3.5
[S II]	6716	2.2	0.6	3.4	0.3	1.0	1.2	6.9	7.8	0.4	0.3
[S II]	6731			4.8	0.7	1.8	2.4	9.4	10.5	0.7	0.6
He I	7065			1.5	6.9	3.9	6.9	2.4	4.7	5.0	9.9
[Ar III]	7136			1.9	5.2	5.1	6.3	6.2	4.6	5.9	5.0
[O II]	7320	26.6	33.5	10.3	27.0	20.2	19.6	8.6	10.8	11.9	15.7
[O II]	7330	14.3	24.9	8.4	21.2	10.9	14.9	7.0	8.2	6.4	12.7

